Simulation for MSS-2 low-perigee elliptical orbit satellites: an example of lithospheric magnetic field modelling

Jiang, Yi; Olsen, Nils; Ou, JiaMing; Yan, Qing

Published in:
Earth and Planetary Physics

Link to article, DOI:
10.26464/epp2023021

Publication date:
2023

Document Version
Publisher's PDF, also known as Version of record

LETTER
PLANETARY SCIENCES

Earth and Planetary Physics
7: 151–160, 2023
doi: 10.26464/epp2023021

Simulation for MSS-2 low-perigee elliptical orbit satellites: an example of lithospheric magnetic field modelling

Yi Jiang[1*], Nils Olsen[2], JiaMing Ou[1], and Qing Yan[1]

[1]State Key Laboratory of Lunar and Planetary Sciences, Macau University of Science and Technology, Taipa 999078, Macao, China;

[2]Division of Geomagnetism, DTU Space, National Space Institute, Technical University of Denmark, Diplomvej 371, 2800 Kgs. Lyngby, Denmark

Key Points:

- The future four-satellite constellation comprising MSS-1 and MSS-2 will enable improved measurements of the geomagnetic field in three dimensions and at previously understudied altitudes.
- We simulate results from elliptical orbits and compare to those from circular satellite orbits.
- Data from MSS-2's elliptical orbits are expected to help improve the accuracy and resolution of lithospheric magnetic field models.

Citation: Jiang,Y., Olsen, N., Ou, J. M., and Yan, Q. (2023). Simulation for MSS-2 low-perigee elliptical orbit satellites: an example of lithospheric magnetic field modelling. *Earth Planet. Phys.*, *7*(1), 151–160. http://doi.org/10.26464/epp2023021

Abstract: A future constellation of at least four geomagnetic satellites (designated Macau Scientific Satellite-1 (MSS-1) and Macau Scientific Satellite-2 (MSS-2)) was recently proposed, to continue high-quality geomagnetic observations in the post-Swarm period, focusing especially on collecting data that will provide a global, three-dimensional survey of the geomagnetic field. In this paper, we present a simulation of two years of orbits (2020.01.01–2022.01.01) of two satellites (tentatively denoted as MSS-2) that are constellated in elliptical (200 × 5,300 km) low-perigee orbits. By comparing error variances of Gauss coefficients, we investigate the sensitivity of lithospheric magnetic field modelling to data collected from various satellite orbits, including a near circular reference orbit of 300 × 350 km, and elliptical orbit of 180 × 5,300 km, 220 × 5,300 km, 200 × 3,000 km and 200 × 1,500 km. We find that in two years the two MSS-2 satellites can collect 35,000 observations at altitude below 250 km, data that will be useful in advancing the quality of lithospheric magnetic field modelling; this number of observations reflects the fact that only 4.5% of the flight time of these satellites will be below 250 km (just 6.4% of their flight time below 300 km). By combining observations from the MSS-2 satellites' elliptical orbits of 200 × 5,300 km with observations from a circular reference orbit, the variance of the geomagnetic model can be reduced by a factor of 285 at spherical harmonic degree n = 200 and by a factor of 1,300 at n = 250. The planned lower perigee of their orbits allows the new satellites to collect data at unprecedentedly lower altitudes, thus dramatically improving the spatial resolution of satellite-derived lithospheric field models, (up to 80% at n=150). In addition, lowering the apogee increases the time interval during which the satellites fly at near-Earth altitudes, thus improving the model predictions at all spherical harmonic degrees (around 52%–62% at n = 150). The upper limit of the expected improvement to the field model at the orbital apogee is not as good as at the perigee. However, data from the MSS-1 orbit can help fill the gap between data from the MSS-2 orbits and from the circular reference orbit for the low-degree part of the model. The feasibility of even lower-altitude flight requires further discussion with satellite engineers.

Keywords: elliptical orbit; satellite orbit simulation; lithosphere field modelling; spherical harmonics

1. Introduction

Modelling the global lithospheric field to high degree of accuracy has been difficult because magnetic field observations with global coverage can be collected only from satellites and are thus restricted by their orbital altitudes. Swarm, the current satellite constellation, has been providing high-precision magnetic field data for ten years since its launch on 22 November 2013 and is expected to continue to do so until at least 2025, well beyond its original expected lifetime of five years.

Correspondence to: Y. Jiang, yjiang@must.edu.mo
Received 03 SEP 2022; Accepted 06 DEC 2022.
Accepted article online 29 DEC 2022.

The Swarm constellation consists of three satellites with near-circular polar orbits. Two of them, Alpha and Charlie, are flying side by side at about 470 km with an inclination 87.4°. The other satellite, Bravo, orbits at the slightly higher altitude of about 520 km with an inclination 88°. Although the difference in east–west (EW) gradients obtained from the unique orbits of the Alpha and Charlie in Swarm and the difference in north–south (NS) gradients from circular polar orbits can improve the resolution of lithospheric magnetic field models, their impact is still limited by the fact that the satellites are at a relatively high altitude and are limited to NS circular orbits.

Data collected at about 280–300 km by the CHAMP (Challenging Minisatellite Payload) satellite two years before it crashed remain the primary data set for global lithospheric magnetic field

modelling. Among models based on CHAMP data, in combination with data from other satellites such as Swarm, Ørsted, and SAC-C, are the CM series of models (Sabaka et al., 2004, 2015, 2020), the CHAOS series (Olsen et al., 2014; Finlay et al., 2015, 2016, 2020), the MF series (Maus et al., 2007, 2008; Maus, 2010), the LCS-1 model (Olsen et al., 2017), and the DLFI-5.2 (Thébault et al., 2021). However, these satellite models are limited to degree 185 (corresponding to horizontal wavelength 216 km) and there are still some unwanted NS-trending features in these models.

In the last five years, China has made significant developments in satellites collecting magnetic field data. A new mission of novel constellation (Zhang K, 2022) is being planned that can offer a higher-precision and three-dimensional survey of the Earth's magnetic field alongside its external three-dimensional magnetic environment. We discuss this project's key scientific research goals and applications.

This novel constellation will include at least four satellites, two in a lower-latitude near-circular orbit with inclination 41°, and two planned to have the same elliptical near-polar orbit of 200 × 5,300 km, but in different orbital planes, allowing the two satellites to fly simultaneously, one in the northern hemisphere and one in the southern. The first step has already been taken: The first magnetic satellite mission, named Macau Science Satellite-1 (MSS-1), is scheduled for launch in 2023. Its main task is to observe the South Atlantic Anomaly (noted as SAA) at ~450 km with an inclination of ~41°. MSS-1 consists of two satellites (A and B). Satellite A, equipped with an absolute scalar magnetometer (produced by IWF (Institut fuer Weltraumforschung)) and two vector field magnetometers installed on its optical bench (VFM (Vector Field Magnetometer) designed by the DTU (Technical University of Denmark), and another developed by the IGG (Institute of Geology and Geophysics, Chinese Academy of Sciences), 0.8 m away from it), is expected to provide the same high-quality data as Swarm. Satellite B is not equipped with instruments related to magnetic measurements.

Two follow-on low perigee elliptical orbit satellites (tentatively denoted as MSS-2) have been planned. Their 200 km perigee is much lower than that of the current CHAMP orbits, so they will be able to collect data over a considerably extended range of altitude. Three-dimensional (EW by MSS-1 and NS by MSS-2) and lower-altitude data will facilitate better modelling precision and resolution of the lithospheric magnetic field. In addition, observations at apogees of up to 5,300 km will provide a better understanding of the ionosphere and the inner magnetosphere. It is anticipated that the new satellite constellation will continue to provide, compared to the Swarm mission, higher quality, and more multi-dimensional geomagnetic measurement perennially in the post-Swarm period, making a significant contribution to the development of high-resolution and high-precision maps of the Earth's magnetic field, and revealing more detail about the various sources of the geomagnetic field, including the core field, the lithospheric field, the ocean tidal field, the ionospheric field, the magnetospheric field, and their induced fields.

Take the lithospheric magnetic field as an example: The lithospheric signal is well retained on the ground, but it decreases rapidly with increasing altitude and increasing degrees of spherical

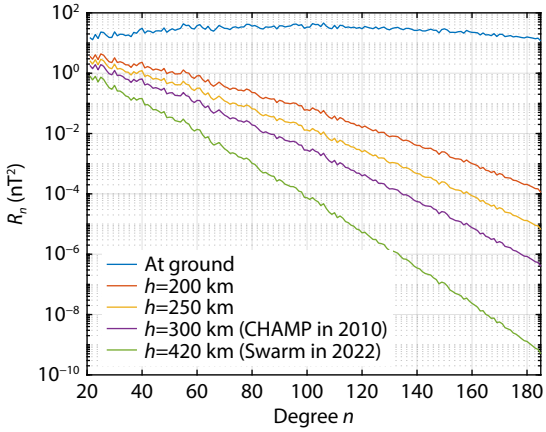

Figure 1. Lowes–Mauersberger power spectrum at different altitude.

harmonics, which can be seen clearly in Figure 1, presents the Lowes–Mauersberger spatial spectrum (Mauersberger, 1956) at different altitudes based on the CHAOS-7 model. Present satellite models can extend formally up to degree 185. On the ground, the power of the lithospheric magnetic field is 'flat' (blue line). But the average power, for example at spherical harmonics degree n = 180, is about 0.85×10^{-8} nT^2 (corresponding to only 0.9 pT for the lithospheric field signal) at 300 km, which was the altitude of CHAMP during the last months of its mission, represent by the purple line. At 420 km (green line), the altitude of Swarm in 2022, the signal is attenuated by 25 times compared to its strength at 300 km. Weak lithospheric magnetic field signals will be hidden in model misfits or mixed with signals from other field sources that are hard to separate in the model, thus compromising accurate study of the lithospheric magnetic field.

In general, detection of a magnetic structure of a given spatial size requires observations made at altitudes equal to or lower than the given spatial size. However due to the resistance of the Earth's atmosphere, most satellites are launched at 300–1500 km with near-circular orbits, because their orbits would otherwise decay rapidly. Satellites collecting magnetic field data usually fly at about 400 km or higher (Magsat at 350–550 km, CHAMP at 350–450 km, Swarm at 450–500 km, Ørsted and SAC-C above 600 km). Exceptions have been CHAMP and GOCE (Gravity field and steady-state Ocean Circulation Explorer) (Drinkwater et al., 2003): CHAMP had descended to a maximum of about 250 km in the last year before the end of its mission; the average altitude for CHAMP data eligible for modelling is around 280–300 km; GOCE, thanks to an innovative electric propulsion system, is one of the closest satellites to Earth, collecting data at about 270 km. Although aeromagnetic data or other near-Earth data sources can partially compensate for lack of satellite observations (Jiang Y et al., 2021) e.g., EMM model (https://geomag.us/models/index.html) can reach to degree 790 and DLFI-5.2 has 1,050 degrees, current models have a gap between horizontal wavelengths 150 to 200 km that data from circular satellite orbits are hardly able to fill.

In contrast, the perigees of the new elliptical orbits will be significantly lower, down almost to 200 km. Orange and yellow lines in Figure 1 describe the spatial spectrum of the lithospheric magnetic field at 200 and 250 km, respectively. The signal

captured at this altitude range is 16 times stronger than at 300 km; these new data will thus provide a good complement to other previously available data sources for lithospheric magnetic field modelling. The orbits of three of the POGO (Polar Orbiting Geophysical Observatory) satellites (POGO 2, 4, 6) provide data that help predict what we can expect from the elliptical orbit of 400 × 1,500 km (Krebs, 2022).

Satellite, magnetometer, and data processing technologies have all come a long way over the past 60 years. Recent advances have made it possible to tackle the challenge of low-altitude data collection that will allow modeling of the lithospheric magnetic field to an extent that has never before been possible. In 2020, European Space Agency (ESA) announced plans for a mission named Daedalus (Sarris et al., 2020; ESA, 2020) that will use ultra-low elliptical satellite orbits; Daedalus is focused on investigating physical processes in the lower thermosphere and ionosphere, e.g., "Joule heating" and related space-weather phenomena, using in-situ measurements at low altitudes. The observation of the magnetometer at 140 × 1,500 km aims to play a very important role in the study of the lithospheric magnetic field (Olsen, 2022).

This paper focuses on the innovation and contribution of large elliptical satellite orbits in collecting improved geomagnetic data; we use lithospheric magnetic field modelling as an example. We present simulations of different satellite orbits, including circular reference orbits and elliptical orbits with different perigees or apogees. We explore how data selection criteria (e.g., nightside of data and geomagnetic quiet conditions) and how different combinations of data sets (e.g., from circular and elliptical orbits) can improve the modelling of the lithospheric magnetic field. Orbit synthesis is described in Section 2. Section 3 presents an analysis and discussion of elliptical orbits. Our conclusions and outlook appear in Section 4.

2. Simulation of Elliptical Orbits of Satellites

2.1 Synthetic Orbits

Satellite orbits are numerically integrated by use of a 12th-order Gauss–Jackson integration scheme. Full details of the method are in Montenbruck et al. (2002). The gravity model used in the synthesis can be written as

$$U = \frac{GM}{r}\sum_{n=0}^{N}\sum_{m=0}^{n}\frac{R^n}{r^n}P_{nm}(\sin\varnothing)\left(C_n^m\cos m\lambda + S_n^m\sin m\lambda\right), \quad (1)$$

in which r is the distance from the satellite to Earth's center. R = 6,378.1366 km is the reference radius of Earth, GM = 398,600.4415 km^3/s^2 is gravitational constant times the Earth's mass; C_n^m and S_n^m are gravity field coefficients up to degree 2; P_{nm} is the associated Legendre polynomial of degree n and order m.

Since the analysis does not require precise satellite positions, the effects of non-gravitational forces are ignored. We also did not consider air drag, assuming that this effect has been compensated for by satellite thruster activity that maintains consistent orbit perigee and apogee throughout the mission.

The elliptical orbit of the two Macau Scientific Satellite-2 (MSS-2) satellites is initially set to be 200 × 5,300 km, inclination 88°, with their initial perigee latitudes at 65°N (MSS-2A) and 65°S (MSS-2B), respectively. Different perigees determine the minimum altitude of data collection; apogee determines the orbital period and therefore the amount and timing of low-altitude data collection. For convenience of comparison, in this paper we calculate other orbits, including elliptical orbits 180 × 5,300 km, 220 × 5,300 km, 200 × 3,000 km, and 200 × 1,500 km, and a circular reference orbit (300 × 350 km), during the period from 1st Jan 2020 to 1st Jan 2022 with sample rate of 30 sec (one sample every 30 sec). Values of right ascension of ascending node Ω and mean anomaly M are set to 0° at the beginning of the period. A simulated four-hour sample result for an MSS constellation is shown in Figure 2. The constellation consists of a circular orbit satellite (MSS-1, blue line) and two elliptical orbit satellites (MSS-2A, red line; MSS-2B, yellow line). Table 1 lists the Kepler elements for the simulated orbit configura-

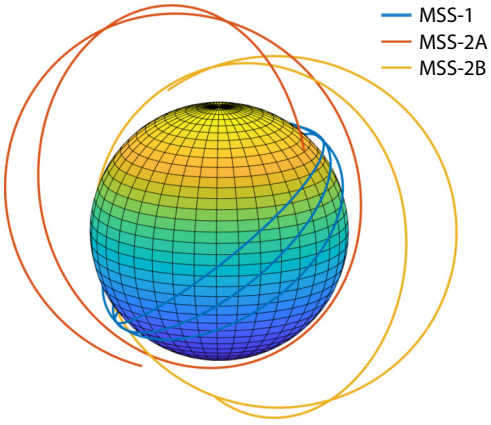

Figure 2. A sample result of Orbital simulation over four hours.

Table 1. Kepler elements for different orbits.

Kepler elements	Orbit 1 MSS-2	Orbit 2 300 × 350 km	Orbit 3 MSS-1	Orbit 4 180 × 5,300 km	Orbit 5 200 × 1,500 km
Perigee altitude, r_p	200 km	300 km	400 km	180 km	200 km
Apogee altitude, r_a	5,300 km	350 km	450 km	5,300 km	1,500 km
Orbit inclination, i	88°	88°	41°	88°	88°
Change of argument of perigee, $\dot{\omega}$	−1.74°/day	−4.36°/day	−4.14°/day	−1.75°/day	−3.40°/day
Semi-major axis, a_{sma}	9,128.1 km	6,703.1 km	6,803.1 km	9,118.1 km	7,228.1 km
Eccentricity, e	0.2794	0.0037	0.0037	0.2808	0.0899
Orbit period, T_{orb}	144.7 min	91 min	93.1 min	144.4 min	101.9 min

tion.

The first two simulations represent the MSS-2 orbit of 200 × 5,300 km (Orbit 1) and near circular reference orbit of 300 × 350 km (Orbit 2), respectively. The MSS-1 orbit simulation (Orbit 3) is also presented in the table; its last two orbits are the elliptical orbit with lower perigee (Orbit 4) and with lower apogee (Orbit 5). Except for MSS-1, with inclination i of 41°, all other orbits have inclinations set to 88°; r_a and r_p are the radii of apogee and perigee, respectively.

The period of a Keplerian orbit (Eq. 2.39 from Montenbruck et al., 2002) is given by

$$T_{\rm orb} = 2\pi\sqrt{\frac{a_{\rm sma}^3}{GM}}, \tag{2}$$

Where $a_{\rm sma} = r_a(1+e)$ is the semi-major axis of the circular reference orbit; orbit eccentricity $e = (r_a - r_p)(r_a + r_p)$.

MSS-2 can provide about 10 orbits every day (its period is approximately 2.5 hours). A 20 km lower perigee does not have much effect on the orbital period. The reduction of apogee from 5,300 to 1,500 km can shorten the orbital period by more than 40 minutes. On the other hand, the period of the near circular reference orbit is about 1.5 hours, corresponding to 16 orbits per day.

Perigee varies throughout the mission, because of the oblateness of Earth, thus allowing access to low-altitude data with global satellite coverage. Figure 3 gives the variation of perigee latitude for two satellites. Blue line is for MSS-2A, perigee starting at 65°N; red line shows the MSS-2B beginning at 65°S. The change of argument of perigee $\dot{\omega}$ is calculated as follow (Eq. 6.20 from Wertz and Larson, 1999):

$$\dot{\omega} = \frac{-3}{4}\sqrt{\frac{GM}{a_{\rm sma}^3}}J_2\left(\frac{R}{a_{\rm sma}}\right)^2\frac{1-5\cos^2 i}{\left(1-e^2\right)^2}, \tag{3}$$

where $J_2 = 1,082.63 \times 10^{-6}$ is the dimensionless geopotential coefficient. The perigee altitude does not change too much over time, so MSS-1 will thus provide data covering ±41°N in about 7 days (before data selection). MSS-2 will traverse all latitudes in about 3 months ($\dot{\omega} = 1.74°$/day), about 7 times in two years. Besides, $\dot{\omega}$ can be improved to about 3.4° per day when apogee drops down to 1,500 km (Orbit 5), corresponding to approximately 53 days.

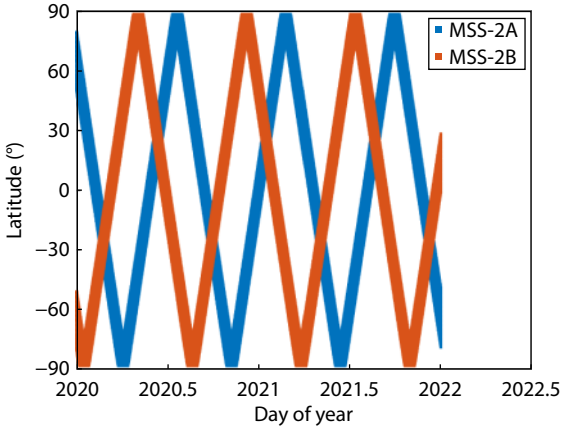

Figure 3. Perigee latitude of MSS-2 varies with year.

From Figure 3 it appears that MSS-2A and MSS-2B do not fly in exactly opposite orbits (by which we mean that whenever one satellite has a perigee at some latitude, the other satellite would be exactly at the other side of the globe). Figure 2 gives the same impression.

In addition, we note in the calculation that due to the Earth's ellipsoidal shape—the difference of 20 km between its equatorial and polar radius—the natural perigee at polar latitudes would be 20 km lower than that at the equator. Such differences can be corrected by satellite operators, which would mean that perigees will probably always be 200 km above surface.

2.2 Flight Time Distribution as a Function of Altitude

The satellite data used in magnetic field modelling are generally collected at about 450–500 km, except for the last year of CHAMP data. Therefore, we focus on data at lower altitudes, i.e., 200–300 km. Unlike Swarm or CSES (China Seismo-Electromagnetic Satellite), the elliptical orbits of MSS-2 satellites will severely limit the amount of time that they will fly at close to perigee altitude. Figure 4 presents the percentages of flight time below different altitudes. The two satellites in the MSS-2 project have the same percentages.

In Figure 4a, we see that MSS-2 (blue line) will spend only about 10% of its flight time below 500 km. Flight time percent increases exponentially with altitude; the percentages for 250 and 300 km are 4.5% and 6.4%, respectively. However, circular reference orbits also collect little data at lower altitudes; the bulk of the data they provide is collected at around 350 (red line) or 450 km (yellow line).

Figure 4b illustrates flight time percentages for elliptical orbits with different perigees. Change of perigee influences the percentage of low-altitude data, an effect that diminishes with increasing altitude. However, for elliptical orbits with different perigees, flight times below 500 km change only modestly. For example, a 20 km reduction in perigee, from 200 to 180 km, can raise time spent at 250 km by 0.8% and at 300 km by 0.6%; a 20 km increase, to 220 km, will cause the same percentages to fall by 1% and 0.7%, respectively.

Figure 4c compares the effects of different apogees. We compare the 5,300 km apogee of the MSS-2 mission to two lower apogees—3,000 km (red line) and 1,500 km (yellow line). Our analysis shows that flight times at target altitudes would be enhanced by 6.9% (at 250 km) and 9.9% (at 300 km) if the apogee were lowered to 3,000 km, and by 11.2% (at 250 km) and 16.1% (at 300 km) if apogee were 1,500 km—that is, flight times 1.5 and 2.5 times higher than the 5,300 km track, respectively. Thus, unlike changes in perigee, changes in apogee can cause the percentage of flight time below 500 km to rise almost to 30%.

Although the MSS-2 satellites will not spend much time flying below 250 km or 300 km, they still can provide enough data for magnetic field modelling, especially because the two MSS-2 satellites collect data simultaneously. According to the statistics in Figures 3 and 4, in three months the two MSS-2 satellites can provide data with global coverage at altitude below 250 km. It

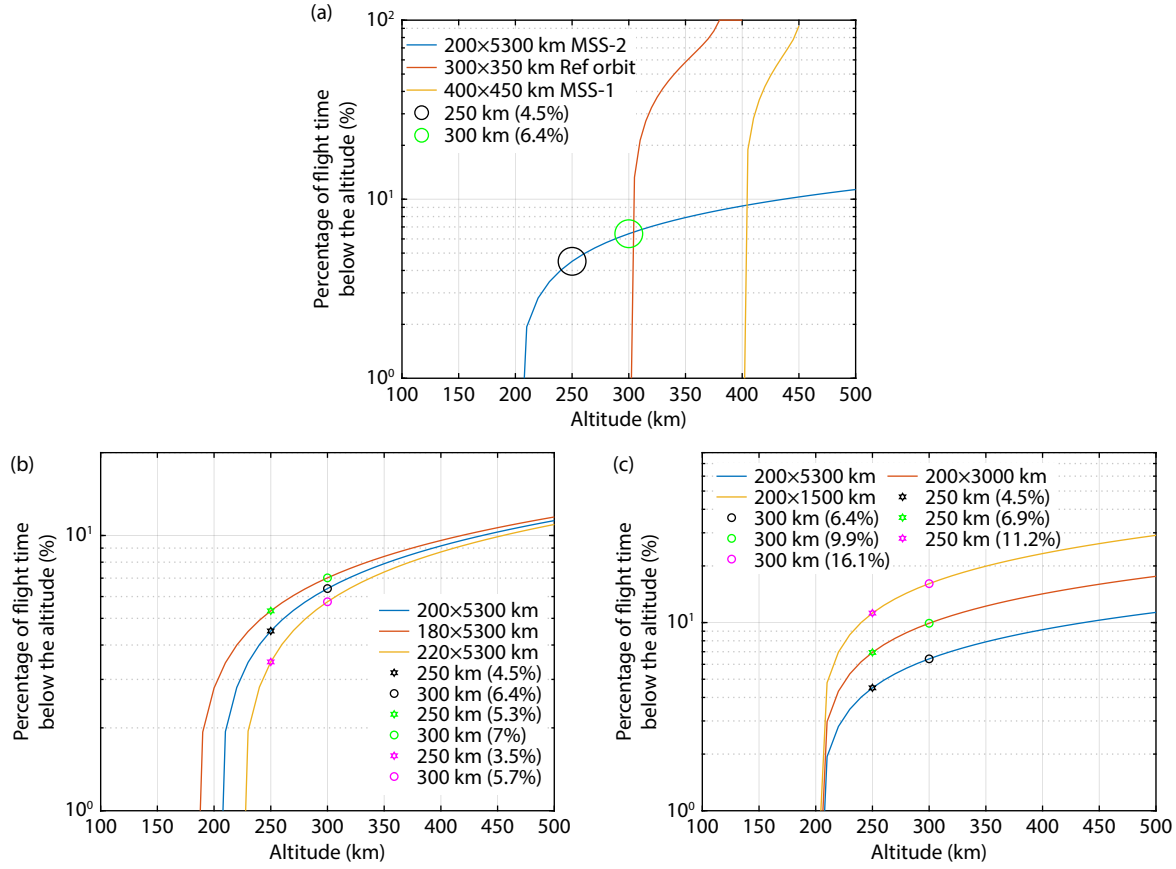

Figure 4. Percentage distribution of flight time below the different altitudes. (a) Comparison between the MSS-2 elliptical orbit (blue; 200 × 5,300 km) and two circular orbit (red: 300 × 350 km; yellow: 400 × 450 km). (b) Comparison among elliptical orbits with different perigees (blue: 200 × 5,300 km; red: 180 × 5,300 km; yellow: 220 × 5,300 km). (c) Comparison between elliptical orbits with different apogees (blue: 200 × 5,300 km; red: 200 × 3,000 km; yellow: 200 × 1,500 km), The orbits of MSS-2A and MSS-2B yield similar percentages.

would take a single satellite at least 190 days to perform the same task.

3. Analysis and Discussion of the Satellite Magnetic Measurements to the Lithospheric Magnetic Field

3.1 Data Selection

In modelling the lithospheric magnetic field, our simulation uses the same selection criteria as was applied to the vector data in the CHAOS-7 and LCS-1 models, i.e., data were selected only from the dark (sun at least 10° below the horizon), and from times when the Ring Current (RC) index changed by at most 2 nT/h and $Kp \leq 2^0$.

Table 2 lists the number of data collected by different simulation tracks from 2020.01.01 to 2022.01.01, filtered by the above criteria. During this period, the selection criteria for *Kp* and RC index will cause nearly half of the data to be rejected, and the screening of night side can retain only roughly 40% of the remaining data. Below 500 km, circular orbits can yield 10 times more magnetic field observations than MSS-2. In contrast, below 250 km more than 35,000 eligible data can be collected by the two satellites in two years. Furthermore, the lower the altitude of the apogee, the

Table 2. Simulation of Number of selected data collected by various orbits in two years.

Orbits	Number of selected data <250 km	Number of selected data <300 km	Number of selected data <500 km
MSS-2A	18,724	26,754	47,615
MSS-2B	17,650	25,149	44,782
MSS-1	—	—	473,210
300 × 350 km	—	499	435,181
180 × 5,300 km	22,261	29,396	49,331
220 × 5,300 km	14,986	24,719	47,412
200 × 3,000 km	28,374	40,657	72,656
200 × 1,500 km	46,663	66,966	121,532

greater the amount of data at these lower altitudes. Lowering the perigee altitude can slightly increase the total amount of data available, but more importantly, significantly more lower altitude data can be obtained. Of course, lowering the perigee would require addressing the challenging engineering problems of flying satellites at low altitudes. In any case, the analysis above suggests that the two MSS-2 satellites will provide enough low-altitude data of global coverage within a year or two to allow construction of a comprehensive global lithospheric field.

3.2 Variances of Gauss Coefficients

Since the lithosphere magnetic field is independent of time, the internal field can be represented as the gradient of a scalar potential ($\boldsymbol{B} = -\nabla \boldsymbol{V}$), with the potential satisfying Laplace's equation $\nabla^2 \boldsymbol{V} = 0$, expanded in spherical harmonics:

$$\boldsymbol{V} = a\left(\frac{a}{r}\right)^{n+1}\sum_{n=1}^{N}\sum_{m=0}^{n}\left[g_n^m \cos m\lambda + h_n^m \sin m\lambda\right]P_n^m(\cos\theta), \quad (4)$$

(Chapman and Bartels, 1940), where a = 6371.2 km is the radius of the Earth, (θ, λ, r) are the geographical coordinate system (colatitude, longitude and spherical radial distance), $\{g_n^m, h_n^m\}$ are the Gauss coefficients and $P_n^m(\cos\theta)$ are the Schmidt semi-normalized associated Legendre functions of degree n and order m. The magnetic field vectors $\boldsymbol{B} = \{B_r, B_\theta, B_\phi\}$ follow as

$$B_r = (n+1)\left(\frac{a}{r}\right)^{n+2}\sum_{n=1}^{N}\sum_{m=0}^{n}\left[g_n^m \cos m\lambda + h_n^m \sin m\lambda\right]P_n^m(\cos\theta), \quad (5a)$$

$$B_\theta = -\left(\frac{a}{r}\right)^{n+2}\sum_{n=1}^{N}\sum_{m=0}^{n}\left[g_n^m \cos m\lambda + h_n^m \sin m\lambda\right]\frac{\partial P_n^m(\cos\theta)}{\partial\theta}, \quad (5b)$$

$$B_\phi = \left(\frac{a}{r}\right)^{n+2}\sum_{n=1}^{N}\sum_{m=0}^{n}\left[g_n^m \cos m\lambda - h_n^m \sin m\lambda\right]\frac{mP_n^m(\cos\theta)}{\sin\theta}. \quad (5c)$$

To estimate the lithospheric magnetic field model coefficients $\{g_n^m, h_n^m\}$, the linear relationship between model and data can be written as

$$\boldsymbol{d} = \boldsymbol{G}\boldsymbol{m}, \quad (6)$$

where $\boldsymbol{d} = \{B_r, B_\theta, B_\phi\}$ are the magnetic field measurements and $\boldsymbol{m} = \{g_n^m, h_n^m\}$ is the model vector for Gauss coefficients. Data kernels matrix $\boldsymbol{G} = \{G_r, G_\theta, G_\phi\}$ is constructed only by the position of the data. Thus, a least-square solution with data error covariance matrix $(\boldsymbol{C}_d)_{ij} = \mathrm{cov}\left((\boldsymbol{d} - \boldsymbol{G}\boldsymbol{m})_i, (\boldsymbol{d} - \boldsymbol{G}\boldsymbol{m})_j\right)$ is expressed as

$$\boldsymbol{m} = \left(\boldsymbol{G}^{\mathrm{T}}\boldsymbol{C}_d^{-1}\boldsymbol{G}\right)^{-1}\boldsymbol{G}^{\mathrm{T}}\boldsymbol{C}_d^{-1}\boldsymbol{d}, \quad (7)$$

(Jenkins and Watts, 1968; Whaler and Gubbins, 1981). The model covariance matrix $\boldsymbol{C}_m$ is given by

$$\boldsymbol{C}_m = \left(\boldsymbol{G}^{\mathrm{T}}\boldsymbol{C}_d^{-1}\boldsymbol{G}\right)^{-1}, \quad (8)$$

Although the Gauss coefficients must be determined by a least-squares fit to the available data, the uncertainty (error) can be estimated without actual data (Olsen et al., 2010). $\boldsymbol{C}_m$ depends only on data position, type and the covariance matrix $\boldsymbol{C}_d$ which rely on the measurement error of the data minus the model values. When the measurement errors are uncorrelated with the same variance σ_d^2 for all data points, then $\boldsymbol{C}_d = \sigma_d^2\boldsymbol{I}$, and model covariance become

$$\boldsymbol{C}_m = \sigma_d^2\left(\boldsymbol{G}^{\mathrm{T}}\boldsymbol{G}\right)^{-1}, \quad (9)$$

where $\boldsymbol{I}$ is a diagonal matrix with elements 1. Given the orthogonality of the spherical harmonics, the normal equation matrix $\boldsymbol{G}^{\mathrm{T}}\boldsymbol{C}_d^{-1}\boldsymbol{G}$ is also a diagonal matrix, if the data distribution is evenly and globally covered (Langel, 1987). Therefore, the model covariance matrix $\boldsymbol{C}_m$ is also a diagonal matrix and its diagonal elements are the variance σ_0^2 of the Gauss coefficients g_n^m, h_n^m.

The global distribution data provided by MSS-2 will be sufficient to build a matrix close to the diagonal matrix, so that its non-diagonal non-zero elements will have negligible effect on the coefficient variance. Therefore, we arbitrarily assume the same error σ_d = 1 nT for all measurement in the simulation.

Figure 5 and Figure 6 demonstrate and compare the variance of Gauss coefficients for various orbits. With respect to quantity of data, every elliptical orbit produces data from two satellites (perigee at 65°N and 65°S), and thus yields better data than from individual satellites. Regardless of circular or elliptical orbits, the error of the model will initially drop with rising spherical harmonic degree until degree 9–14 (Core field dominance), but then will gradually blow up with growing degree.

In Figures 5a and 5b, the circular orbit (yellow line) has a lower variance than the MSS-2 (blue line) orbit, until degree 14. However above degree 14 (at which the lithospheric magnetic field becomes dominant), the variance of MSS-2 data grows significantly slower than that from the circular orbit and is about 150 times smaller at n = 180, 285 times at n = 200, and 1,300 times smaller at n = 250. Furthermore, combining the measurements from MSS-2 + MSS-1 (red line) not only maintains the high accuracy of the lithospheric field, but also compensates for the error of the elliptical orbit in the core field. In addition, Figures 5c, 5d illustrate how changes in perigee and apogee affect model variance. For perigee altitude changes, the impact is relatively small at the beginning, but the difference starts to increase with growing degree due to the lower data collection altitude. The model shows similar improvement (green and pink lines in Figure 5c) when the perigee is lowered from 220 to 200 km, and from 200 to 180 km—improvement of up to about 4.5 times at degree 250. On the other hand, the effect of decreasing the apogee altitude does not change with increasing degree (pink and green line in Figure 5d). A model's accuracy can be improved by a factor of 1.6 when the apogee is lowered from 5,300 km (blue) to 3,000 km (red), and enhanced 2.5 times, compared to the 5,300 km apogee, when lowered to 1,500 km (yellow).

Figure 6 shows the distribution of variance $\sigma_{g,h}^2$ on spherical harmonic degree n and order m for circular (left) and elliptical (right) orbits, respectively (shown only up to degree 250. Above 250, the variance gradually increases). The $\sigma_{g,h}^2$ is a relative value with an arbitrary unit from coefficient variance σ^2 divided by a reference variance (σ_0^2 = 1 nT^2). The g_n^m refers by $m \geq 0$ on the right half, and $m < 0$ refers to h_n^m on the left half. The variance is represented by blue to yellow from small to large.

Variance $\sigma_{g,h}^2$ for a model based on vector data from reference circular orbits are shown in Figure 6a. Figure 6b presents model variance produced by vector data from MSS-2. It is obvious that the low-altitude MSS-2 data can significantly improve the litho-

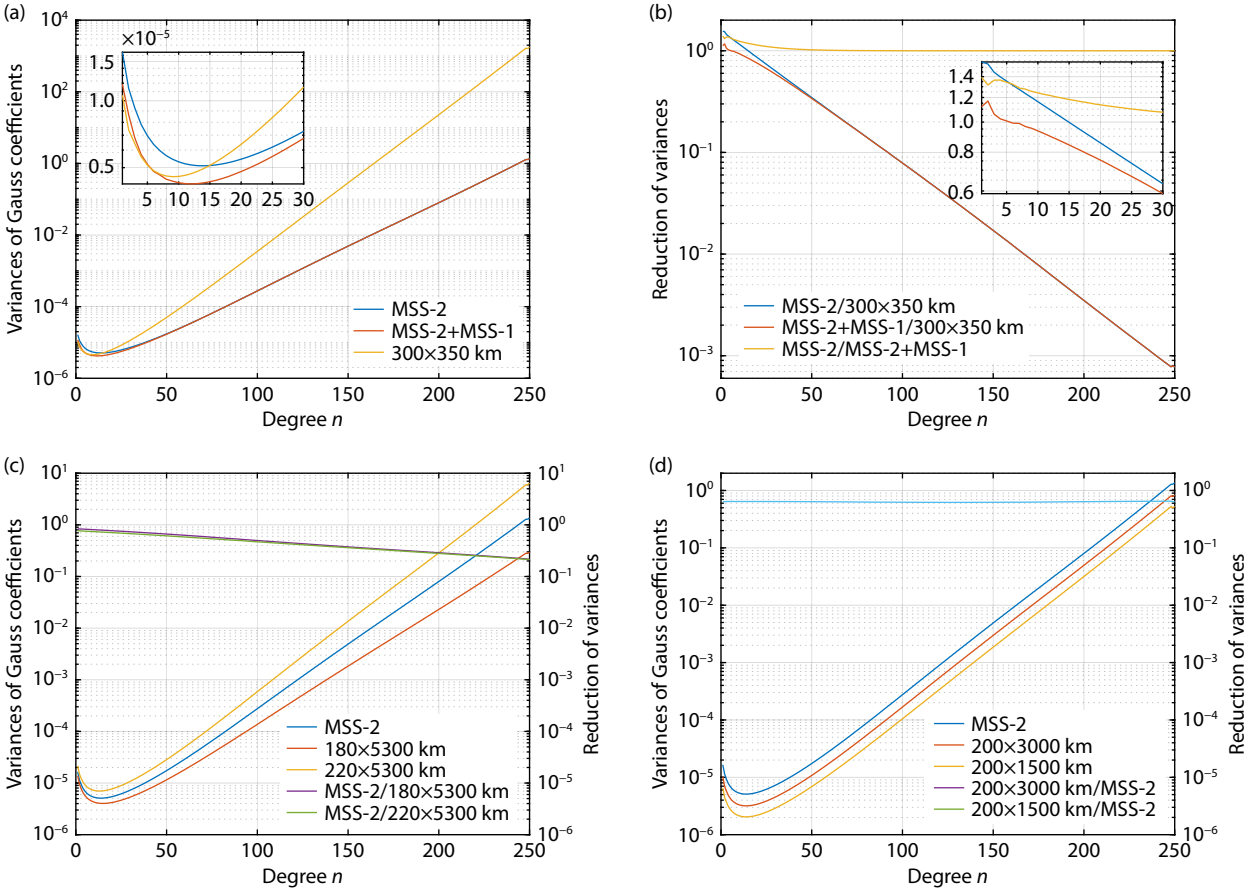

Figure 5. Variance of Gauss coefficients g_1^0 and comparison between different orbits. (a) Variance of Gauss coefficients when using different data set: MSS-2 (blue line), MSS-2+MSS-1 (red line) and 300 × 350 km circular reference orbits (yellow line). (b) Reduction of variance between different data sets: reduction between MSS-2 and circular orbit (blue line), MSS-2+MSS-1 and circular orbit (red line), MSS-2 and MSS-2+MSS-1 (yellow line). (c) Variance of Gauss coefficients when using data from elliptical orbits with different perigees, and the reduction between different variances: variances of MSS-2 (blue), variances of 180 × 5,300 km (red), variances of 220 × 5,300 km (yellow), variance ratio between MSS-2 and 180 × 5,300 km (pink), variance ratio between MSS-2 and 220 × 5,300 km (green). (d) Variance of Gauss coefficients when using data from elliptical orbits with different apogee, and the reduction between different variances: variances of MSS-2 (blue), variances of 200 × 3,000 km (red), variances of 200 × 1,500 km (yellow), variance ratio between MSS-2 and 200 × 3,000 km (pink), variance ratio between MSS-2 and 200 × 1,500 km (green).

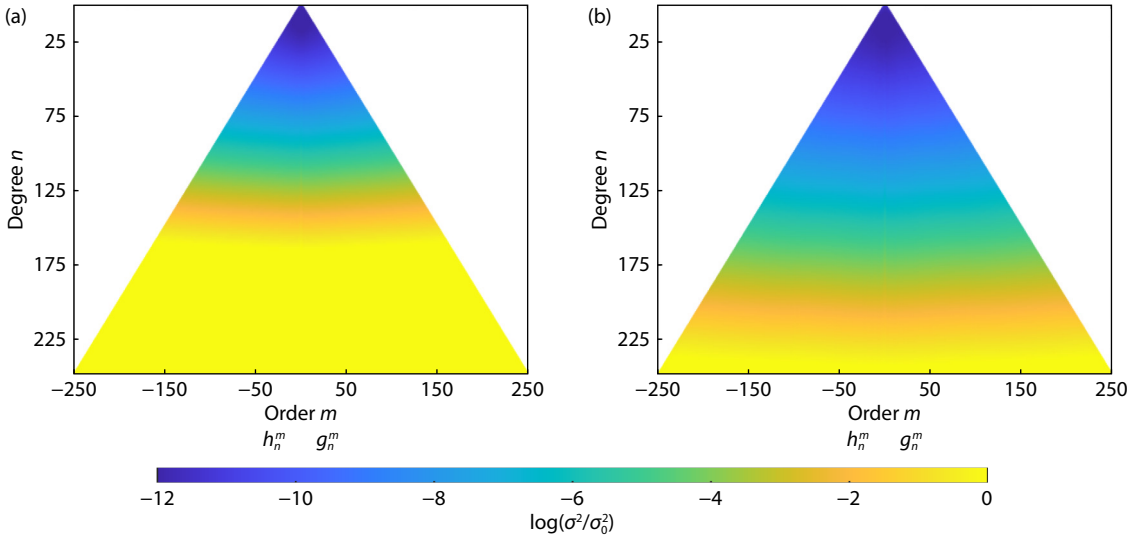

Figure 6. Variance of the spherical harmonic expansion coefficients g_n^m, h_n^m for circular (a) and elliptical (b) orbits from n = 1 to 250.

spheric field model, especially above $n = 100$. The variance distributions of other elliptical orbits in Figure 5 resemble those in Figure 6b.

Figure 7 displays variance ratios between different data sets. A value of that ratio close to 1 indicates no improvement; values below 1 represent potential model improvement.

Figures 7a and 7b present coefficient variances of MSS-2 and MSS-2+MSS-1, respectively, divided by the variances of a circular orbit (the reference model). A ratio less than 1 indicates a greater boost; more than 1 (deep red) means no improvement. Obvious improvement can be seen for all high spherical harmonic degrees (i.e., $n > 20$). However, variance ratios for most of the low-degree coefficients (i.e., $n < 15$) are greater than 1. Exceptions are low-degree near-sectoral (order $m \approx n$) coefficients, which have an amelioration after combining with the MSS-1 data. This may be because MSS-1's orbital inclination $i = 41°$, the gap of half angle $|90° - i| = 49°$, will create difficulties in proper determination of coefficients close to near-zonal term (order $m \approx 0$).

Furthermore, considering past gradient data (Olsen et al., 2017), although the altitude of MSS-1 is rather high compared to the altitude of other orbits, it provides gradient data that might be improved to an even larger degree than suggested by the variance reduction shown in the figure. As the first geomagnetic satellite in an east–west orbit, which has never been done before, its gradient data (compared to data from satellites such as Alpha and Charlie of Swarm) are less affected by remaining external field contamination.

Figures 7c and 7d displays results for 180 × 5,300 km and 200 ×

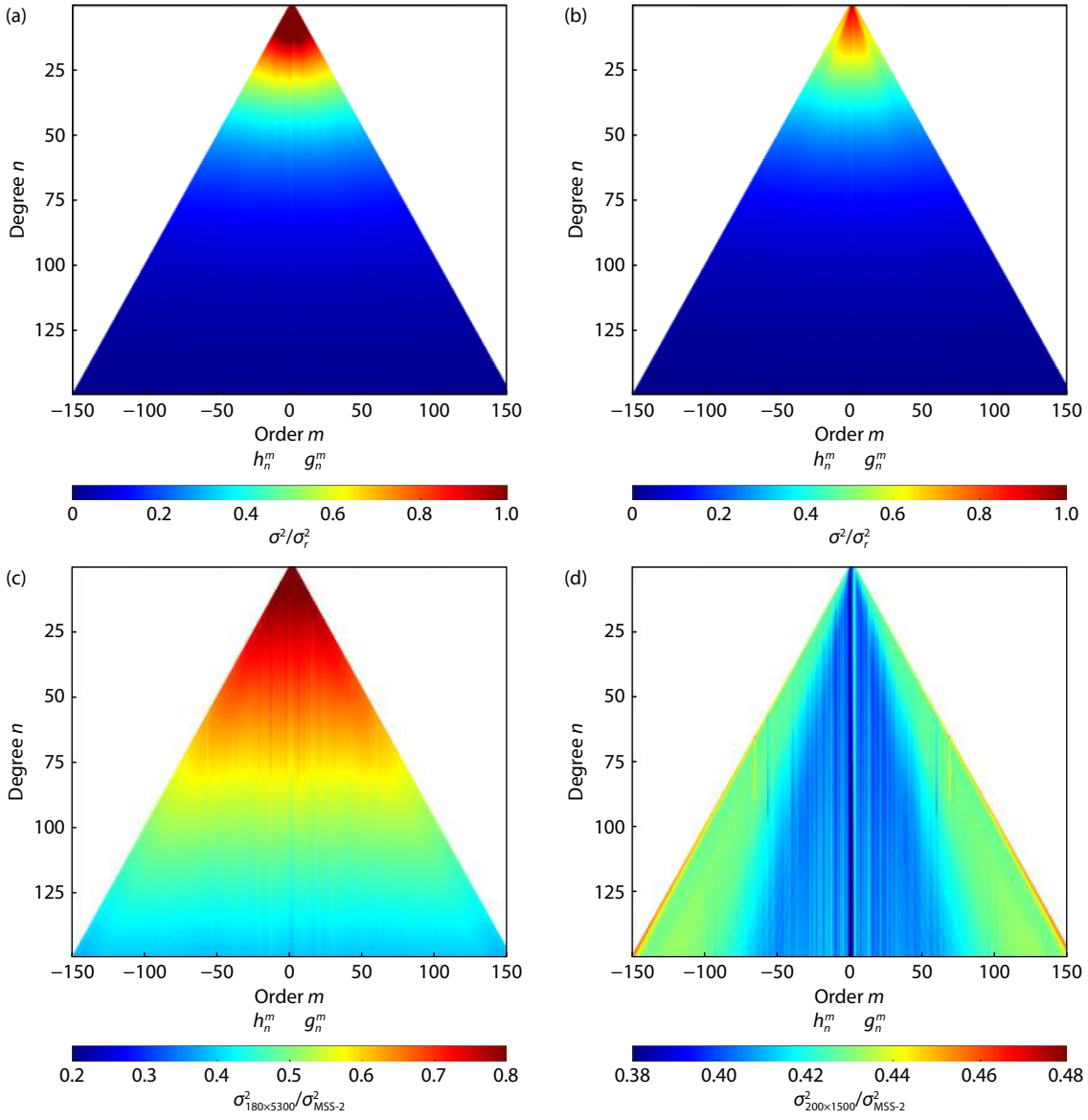

Figure 7. Comparison of variance ratios for models estimated from different orbits. (a) The improvement of model when using MSS-2 data compared to circular orbit data. (b) The improvement of model when using data for MSS-2 + MSS-1 compared to circular orbit data. (c) The improvement of model when using data for 180 × 5,300 km orbit compared to MSS-2. (d) The improvement of model when using data for 200 × 1,500 km orbit compared to MSS-2.

1,500 km orbits, and the reference orbit is that of MSS-2. Lowering the perigee by 20 km can improve the model by at least 20% at low-degree ($n < 40$), and by 50% or more for high-degree ($n > 80$). The apogee is more variable than perigee, which offers more and different improvement for the model. Variance improves to above 50% for all degrees $n \leq 150$. The ratios of near-sectoral terms (order m close to 0) are slightly better than those of near-zonal terms. We conclude that elliptical orbiting satellites with lower perigees and apogees are potentially useful tools in investigation the lithospheric magnetic field.

4. Conclusions and Outlook

Our findings are very encouraging for future magnetic field analysis: the new satellite constellation will collect three-dimensional observations of the geomagnetic field from east–west (EW by MSS-1) and north–south (NS by MSS-2) directions. Several satellites in the constellation complement each other through their respective strengths and can continue to provide high quality geomagnetic survey data with global coverage in the post-Swarm period. These new data collecting systems are expected to make significant contributions to the development of high-resolution and high-precision maps of the Earth's magnetic field, revealing more detail about the various sources of the geomagnetic field, including the core field, the lithospheric field, ocean tidal field, the ionospheric field, the magnetospheric field, and their induced fields.

Compared to previous circular orbiting satellites flying in a NS polar trend, this new satellite constellation not only helps to resolve the unwanted NS-trending features in existing lithospheric magnetic field models (e.g., LCS-1 model), but also allows further improvement of the spatial resolution of the lithospheric magnetic field with low altitude 'gradient' data at low perigee. On the other hand, the observations collected at its high altitude reflect the external three-dimensional magnetic environment, including the magnetic activity of the ionosphere and the inner magnetosphere. Combined with the rapid local time variability of the MSS-1 data, these new data can further enhance understanding of the external field achieved by existing models, provided that the new constellation can deliver magnetic data of the same quality as Swarm and that good consistency can be achieved between different datasets.

We have presented two-year simulations of various satellite orbits, investigating the influence of different satellite orbits on collection of data relevant to lithospheric magnetic field modelling. This sensitivity analysis of low-altitude data to lithospheric magnetic field modelling is done by estimating error variances of Gauss coefficients.

Our findings suggest that in two years the MSS-2 satellite can provide sufficient low-altitude data, despite the fact that only 4.5% of its flight time is below 250 km, and that approximately 80% of the data will be further filtered out due to factors such as *Kp*, RC index, and dark side considerations. In addition, we find that the limited flight time at these lower altitudes is more than compensated for by the much larger crustal signal at low altitudes.

We conclude that low-altitude elliptical orbits provide great improvement for lithospheric magnetic field data collection, compared to circular orbits. Their advantages become more apparent as the spherical harmonic degree increases. Between the MSS-2 orbit of 200 × 5,300 km and circular reference orbit of 300 × 350 km, the variance of the model can be reduced 285 times at $n = 200$ and 1,300 times at $n = 250$. Lowering its orbital perigee allows the satellite to reach lower altitudes, thus improving model predictions at the higher harmonic degrees (up to 80% at $n = 150$). Lowering orbital apogee can increase the time interval when the satellites fly at near-Earth altitudes, thus improving the model at all harmonic degrees (around 52%–62% at $n = 150$). The upper limit of the improvements brought by apogee lowering is not as high as for perigee lowering.

Low altitude vector data are essential to determining the complete global lithospheric field. Lower perigees will make possible collection of magnetic data at lower altitudes, thereby increasing the resolution of the model. And lower apogees can increase the quantity of such data, reducing model error caused by shorter orbital periods. We have not yet performed an end-to-end simulation for the whole MSS-2 mission. Moreover, engineers must be consulted regarding the feasibility of flying satellites at such low altitudes.

Acknowledgments

Y Jiang is supported by the Macau Foundation, Macau Science and Technology Development Fund (Macau SAR 0001/2019/A1, SKL-LPS (MUST)-2021–2023), the National Natural Science Foundation of China (42250101) and by the Pre-research Project on Civil Aerospace Technologies No. D020303/D020308 funded by China National Space Administration.

References

Chapman, S., and Bartels, J. (1940). *Geomagnetism*. Oxford: Oxford University Press.

Drinkwater, M. R., Floberghagen, R., Haagmans, R., Muzi, D., and Popescu, A. (2003). VII: CLOSING SESSION: GOCE: ESA's first earth explorer core mission. *Space Sci. Rev.*, *108*(1), 419–432. https://doi.org/10.1023/A:1026104216284

ESA. (2020). Report for assessment: Earth Explorer 10 Candidate Mission Daedalus, Tech. Rep. ESA-EOPSM-DAED-RP-3793, European Space Agency, Noordwijk, The Netherlands.

Finlay, C. C., Olsen, N., and Tøffner-Clausen, L. (2015). DTU candidate field models for IGRF-12 and the CHAOS-5 geomagnetic field model. *Earth Planets Space*, *67*, 114. https://doi.org/10.1186/s40623-015-0274-3

Finlay, C. C., Olsen, N., Kotsiaros, S., Gillet, N., and Tøffner-Clausen, L. (2016). Recent geomagnetic secular variation from Swarm and ground observatories as estimated in the CHAOS-6 geomagnetic field model. *Earth Planets Space*, *68*(1), 112. https://doi.org/10.1186/s40623-016-0486-1

Finlay, C. C., Kloss, C., Olsen, N., Hammer, M. D., Tøffner-Clausen, L., Grayver, A., and Kuvshinov, A. (2020). The CHAOS-7 geomagnetic field model and observed changes in the South Atlantic Anomaly. *Earth Planets Space*, *72*, 156. https://doi.org/10.1186/s40623-020-01252-9

Jenkins, G. M., and Watts, D. G. (1968). *Spectral Analysis and its Applications*. San Francisco: Holden Day.

Jiang, Y., Holme, R., Xiong, S. Q., Jiang, Y., Feng, Y., and Yang, H. (2021). Long-wavelength lithospheric magnetic field of China. *Geophys. J. Int.*, *224*(3), 1780–1792. https://doi.org/10.1093/gji/ggaa490

Krebs, G. D. (2022). "OGO 1, 2, 3, 4, 5, 6 (EGO 1, 2, 3 / POGO 1, 2, 3)". *Gunter's Space Page*. Retrieved September 01, from https://space.skyrocket.de/doc_sdat/ogo.htm

Langel, R. A. (1987). The main field. In J. A. Jacobs (Ed.). *Geomagnetism*, *1*, 249–512). London: Academic Press.

Mauersberger, P. (1956). Das Mittel der Energiedichte des Geomagnetischen Hauptfeldes an der Erdoberflache und seine säkulare Änderung. *Gerlands Beitr. Geophys.*, *65*, 207–215.

Maus, S., Yin, F., Lühr, H., Manoj, C., Rother, M., Rauberg, J., Michaelis, I., Stolle, C., and Müller, R. D. (2008). Resolution of direction of oceanic magnetic lineations by the sixth-generation lithospheric magnetic field model from CHAMP satellite magnetic measurements. *Geochem. Geophys. Geosyst.*, *9*(7), Q07021. https://doi.org/10.1029/2008GC001949

Maus, S. (2010). Magnetic field model MF7. https://www.geomag.us/models/MF7.html

Maus, S., Lühr, H., Rother, M., Hemant, K., Balasis, G., Ritter, P., and Stolle, C. (2007). Fifth-generation lithospheric magnetic field model from CHAMP satellite measurements. *Geochem. Geophys. Geosyst.*, *8*(5), Q05013. https://doi.org/10.1029/2006GC001521

Montenbruck, O., Gill, E., and Lutze, F. (2002). Satellite orbits: models, methods, and applications. *Appl. Mech. Rev.*, *55*(2), B27–B28. https://doi.org/10.1115/1.1451162

Olsen, N., Hulot, G., and Sabaka, T. J. (2010). Measuring the Earth's magnetic field from space: concepts of past, present and future missions. *Space Sci. Rev.*, *155*, 65–93. https://doi.org/10.1007/s11214-010-9676-5

Olsen, N., Lühr, H., Finlay, C. C., Sabaka, T. J., Michaelis, I., Rauberg, J., and Tøffner-Clausen, L. (2014). The CHAOS-4 geomagnetic field model. *Geophys. J. Int.*, *197*(2), 815–827. https://doi.org/10.1093/gji/ggu033

Olsen, N., Ravat, D., Finlay, C. C., and Kother, L. K. (2017). LCS-1: a high-resolution global model of the lithospheric magnetic field derived from CHAMP and Swarm satellite observations. *Geophys. J. Int.*, *211*(3), 1461–1477. https://doi.org/10.1093/gji/ggx381

Olsen, N. (2022). Modelling Earth's lithospheric magnetic field using satellites in low-perigee elliptical orbits. *Geophys. J. Int.*, *232*(3), 2035–2048. https://doi.org/10.1093/gji/ggac422

Sabaka, T. J., Olsen, N., and Purucker, M. E. (2004). Extending comprehensive models of the Earth's magnetic field with Ørsted and CHAMP data. *Geophys. J. Int.*, *159*(2), 521–547. https://doi.org/10.1111/j.1365-246X.2004.02421.x

Sabaka, T. J., Olsen, N., Tyler, R. H.,and Kuvshinov, A. (2015). CM5, a pre-Swarm comprehensive geomagnetic field model derived from over 12-yr of CHAMP, Ørsted, SAC-C and observatory data. *Geophys. J. Int.*, *200*(3), 1596–1626. https://doi.org/10.1093/gji/ggu493

Sabaka, T. J., Tøffner-Clausen, L., Olsen, N., and Finlay, C. C. (2020). CM6: a comprehensive geomagnetic field model derived from both CHAMP and Swarm satellite observations. *Earth Planets Space*, *72*, 80. https://doi.org/10.1186/s40623-020-01210-5

Sarris, T. E., Talaat, E. R., Palmroth, M., Dandouras, I., Armandillo, E., Kervalishvili, G., Buchert, S., Tourgaidis, S., Malaspina, D. M., … Aikio, A. (2020). Daedalus: a low-flying spacecraft for in situ exploration of the lower thermosphere-ionosphere. *Geosci. Instrum. Methods Data Syst.*, *9*(1), 153–191. https://doi.org/10.5194/gi-9-153-2020

Thébault, E., Hulot, G., Langlais, B., and Vigneron, P. (2021). A spherical harmonic model of Earth's lithospheric magnetic field up to degree 1050. Geophys. *Res. Lett.*, *48*(21), e2021GL095147. https://doi.org/10.1029/2021gl095147

Wertz, J. R., and Larson, W. J. (1999). Space Mission Analysis and Design (3rd ed). Dordrecht: Springer.

Whaler, K. A., and Gubbins, D. (1981). Spherical harmonic analysis of the geomagnetic field: an example of a linear inverse problem. *Geophys. J. Roy. Astr. Soc.*, *65*(3), 645–693. https://doi.org/10.1111/j.1365-246X.1981.tb04877.x

Zhang, K. (2023). A novel geomagnetic satellite constellation: Science and applications. *Earth Planet. Phys.*, *7*(1), 4–21. https://doi.org/10.26464/epp2023019